# NTNU

Institutt for energi-
og prosessteknikk

# SINTEF

# Bacheloroppgave

| | |
|---|---|
| **Oppgavens tittel:** | **Gitt dato:** 20.12.2022 |
| Effekten marin atmosfærisk strømning under ekstreme vindforhold har på flytende PV system | **Innleveringsdato:** 22.05.2023 |
| | **Antall sider rapport / sider vedlagt:** |
| **Project title (ENG):** | |
| Effect of marine atmospheric flow under extreme wind-wave conditions on floating PV systems | 31/44 |
| **Gruppedeltakere:** | **Veileder:** Tania Bracchi |
| Håvard Haugland, Andreas Vaage, Ole Sebastian Holltrø Søraas | **Prosjektnummer:** BIFOREN23-11 |
| **Oppdragsgiver:** | **Kontaktperson hos oppdragsgiver:** Balram Panjwani |
| SINTEF | |

Fritt tilgjengelig: ☐

Tilgjengelig etter avtale med oppdragsgiver: ☑

Rapporten frigitt etter:

**Gruppedeltakere signaturer:**

*Håvard Haugland*

*Sebastian Søraas*

*Andreas Vaage*

# NTNU
Kunnskap for en bedre verden

## FAKULTET FOR INGENIØRVITENSKAP

### FENT2900 - BACHELOROPPGAVE
### FORNYBAR ENERGI

# Effect of marine atmospheric flow under extreme wind-wave conditions on floating PV systems

*Forfattere:* Ole Sebastian Holltrø Søraas, Håvard Haugland og Andreas Vaage

2023 Vår

# 1 Preface

This Bachelor thesis was done during the 2023 spring session at NTNU, Norges Tekniske-Naturvitenskapelige Universitet, in collaboration with SINTEF. The completion of this thesis ends the 3-year Bachelor study for Renewable Energy at NTNU. The Bachelor project has given a great understanding of wind forces and their effects on floating solar panels, FPV, in open waters, and simulation of airfoils, as well as flat plates by using BlueCFD, Paraview, and Apame. The project has given a great understanding of how Apame and blueCFD work and the potential weaknesses and strengths of both programs. We would like to thank our supervisor for this project, Balram Panjwani from SINTEF for providing helpful literature and guidance for the simulation programs. We would also like to thank our supervisor from NTNU, Tania Bracchi for giving great help in theory and logistics in this project.

# 2    Abstract

Solar energy is a promising renewable energy alternative. Floating PV systems are a good alternative to land-based PV systems, as it requires less dry land area, and it receives cooling from surrounding water. One problem with FPV systems is that they are prone to damage due to extreme weather conditions. This study aimed to simulate wind loads on FPV systems, using both CFD and the panel method through Apame, and to compare these methods to find out if Apame is a viable option for rough estimates for pressure and lift and drag forces. Apame is a good alternative for rough estimates as it simulates and computes forces at a much faster rate than CFD simulations. In this study, different methods and mesh types in Apame have been used to try to find a consistent and sufficiently accurate way to calculate forces. This was done through multiple different cases simulated in Apame and compared to literature and CFD results, concluding that the First Order Accurate method gave the best lift and drag results as well as pressure results across all cases, and that tilting the mesh before simulating gives more reliable results than Apames tilt function. A 4x4 FPV system mesh has been simulated in both Apame and CFD using First Order and Nodal methods obtaining lift and drag forces and a pressure plot visualized and presented in Paraview. The results showed that the panel method could be a viable time-saving addition to the R&D process provided it is used within the limitation of the method.

# 3    Sammendrag

Solenergi har vist seg å være en låvende fornybar energikilde. Flytende solcellesystemer er et godt alternativ til landbaserte solcellesystemer ettersom de krever mindre landområde og har høyere effektivitet på grunn av at de blir avkjølt av vannet. Flytende solcellesystemer er derimot utsatt for potensielle skader på grunn av ekstreme vind- og værforhold. Dette prosjektet har som mål å simulere hvordan ulike vindhastigheter påvirker solcellesystemene ved å bruke CFD og 3D-panelmetoden i Apame. I tillegg til å undersøke om Apame er et godt nok program for å estimere vindkrefter ved å sammenligne resultatene opp mot CFD metoden og andre raporter. Gjennom prosjektet har det blitt brukt flere beregningsmetoder og varierende meshtyper i Apame for å fastslå hva som gir best resultater ved simulering. Derav ble det konkludert med at First Order Accurate metoden ga mest nøyaktige svar om vindkreftene for alle meshtyper, og at å vippe meshene før simuleringen ga mer presise svar enn å vippe meshen gjennom Apame. Tislutt så har et 4x4 solcellesystem blitt simulert i både Apame og CFD ved å bruke First Order Accurate og Nodal Approximate metoden for å få resultater om løft- og dragreftene i tillegg til kreftene for trykket på solcellesystemet. Kreftene for trykk fra både CFD og Apame har blitt simulert i Paraview for å gi et godt bilde av hvor det er mest og minst trykk på platene. Helhetlig ble det konkludert med at First Order metoden i Apame er et godt verktøy i forskning og utviklings fasen, dersom svakhetene i metoden er tatt til høyde for. Det vil gjøre det mulig å spare vesentlig tid i CFD simulering på grunn av panelmetodens raske simulering.

# Contents

# 4    Introduction

The world today is faced with a huge threat of global warming due to emissions from fossil fuels, which still is the biggest source of heat and electricity. By following the principles of the Paris Agreement to cut all greenhouse gas emissions by 2050, an EU project for floating solar power in the North Sea was created. This European Union-funded project was given to SINTEF, with the goal of developing a FPV system that can withstand winds over $25m/s$.

Solar energy has the capacity to cover all of the globe's energy needs many times greater than the initial required demand. By now the average solar panel efficiency varies around 20% with a lifespan of up to 30 years. Although solar panels and solar energy have existed for a long period of time, it is too insufficient and requires big land areas to make up for the lack of efficiency. New technology has emerged on the scene in recent years, such as a floating solar panel, more precisely called Floating Photo-Voltaic (FPV), and is said to be a better solution for solar power.

Some pros to floating solar panels, compared to regular land-based solar panels are less mainland occupancy, reduced water evaporation in dams, and higher efficiency due to cooling from the surrounding water. A study was given out by Barnard, M [2] stating that the floating solar panels' efficiency stationed above pumped-storage hydropower reservoirs would increase up to 10% due to water cooling.

It does, however, have a higher installation cost compared to PV systems built on land, and it faces problems in damages from wind forces, especially in more open-sea areas than in land-locked areas. Chances for potential damages are possible to reduce by adding wind sheltering walls and blockades between the solar panels.

A solar FPV system consists of multiple solar panels with different inclination angles. These panels are prone to extreme wind loads, such as hurricanes or typhoons. FPV is in the early research and development (R&D) stage when it comes to open sea deployment, and more developments are needed. Deployment of these FPV systems becomes more challenging in the North Sea conditions where the frequency of extreme wind is much higher than in the land-locked systems such as lakes and rivers. Therefore, to ensure the proper functioning of the PV system, it is important to understand the aerodynamic characteristics of the complete FPV system.

The main objective of the thesis is to gain a greater understanding of the wind forces affecting the FPV system, through different calculation programs, and how the program can support different steps in the R&D process. Where flat plates will be used in the programs to simulate solar PV panels and the forces affecting the FPV system.

# 5 Theory

## 5.1 Wind characteristics

The wind speed phenomenon varies over time and height above ground and sea surface. Due to this constant change, an average wind speed time and a reference height need to be determined. The most commonly used height reference point is H = 10m, and 1 minute, 10 minutes, or 1 hour is used for the average wind speed [7]. An 8-year research of wind speed observations on the North Sea coast showed a 7.8 m/s mean wind speed at a height of 18.5 m and a mean wind speed of 7.6 m/s at 15 m [6]. This was done at two different coast locations in the North Sea where the FPV system in this study could be constructed.

The North Sea experiences hurricanes, typhoons, and cyclones regularly. The mean wind speeds for a height of 10 m are not intended to cover these tropical storms. Thus, the mean wind speed needs to be determined by actual on-site storm data, and based on previous recorded on-site data for the wind speed.

Historical wind data gathered from the North Sea by meteoblue [12] over a 30-year duration from 1985-2014 showed that 10.2 days throughout the year experience a wind speed of 16.96 m/s or greater. Another wind database, Windy.app [20], collected over the course of 10 years from 2012 to 2022 showed 15% of the days in the winter months experienced wind speed at 17.99 m/s or greater, 7-10% of the autumn months, and 5-10% of the spring months, with the summer months experiencing calmer wind. Meteoblue [12], showing the same increased wind tendencies in the winter, states that this is due to monsoons where the cold harsh weather in autumn, winter, and fall collide with tropical storms causing greater air pressure differences and more wind. [12].

Research done for numerical simulations of wind loading on floating photovoltaic systems [9] with a 15°tilt, showed that the first row of PV arrays facing the wind would experience the most wind load out of the entire system. Their research was based on an inlet wind velocity of 45 m/s and it showed that the other rows of PV arrays would experience less than half of the inlet velocity, pressure, and lift and drag coefficients compared to the PV arrays on the first row. Their study was done using computational fluid dynamics (CFD) [9]. The shielding effect happens because of the disruption of the boundary layer.

The boundary layer is a thin layer between the airflow and the surface of the flat plate. For each layer inside the boundary layer towards the surface, the velocity moves at a slower rate, till it almost becomes virtually motionless at the surface. The airflow at the top of the boundary layer and on the out-

side moves at a velocity called free-stream velocity 1. The wind speed inside the boundary layer and the free-stream velocity depends on the shape of the body, and other factors such as the viscosity. The airflow inside the boundary layer is called steady flow or laminar flow. When the flow moves more toward the center of the flat plate, and the flat plate vertically increases, the airflow becomes more turbulent, due to friction on the surface 1. Turbulent flow can be expressed by the Reynolds number, $Re_x$:

$$Re_x = \frac{\rho \cdot U_\infty \cdot x}{\mu} \tag{1}$$

where x represents the length of the flat plate, $\rho$ is the density of the airflow, $U_\infty$ is the airflow velocity and $\mu$ is the dynamic viscosity of the airflow. In other words, the inertial forces are divided by the viscous forces, and with higher viscosity, more inertial forces are required to achieve turbulent conditions.

As the flat plate reaches a higher angle of attack, it reaches a certain point where the boundary layer no longer can stay attached to the surface, and instead "lift off" or separation from the surface occurs, at what's called boundary-layer separation. This phenomenon happens when the flat plate has reached its stall point, and the airflow on the upper surface becomes much more turbulent and causes a decrease in lift and an increase in drag [14].
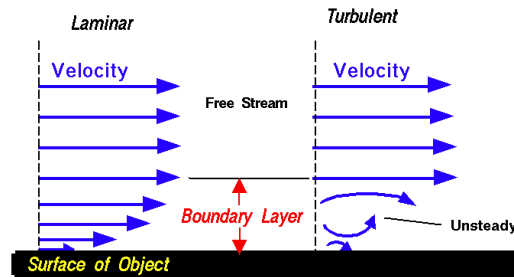


Figure 1: Illustration of the boundary layer [3]

The stall or stalling in terms of aerodynamics is the position for an airfoil to reach maximum lift based on the wind velocity, before boundary-layer separation. After boundary-layer separation occurs the lift starts to decrease with each angle of attack, slowly reaching zero lift. In regards to a flat plate, the stalling point occurs at a much lower angle of attack due to similarity design for the upper and lower surfaces, and having a "non-smooth" leading edge. The wind flowing at the upper and lower surfaces doesn't re-attach after the leading edge 2, and instead, a turbulent flow (wake) appears on the upper surface of the flat plate. The wake will change the flow behind the flat plate, making it more turbulent [19]. This will cause the forces on the following flat

3

plate to change because it is affected by a different flow. That pattern is followed every time objects are closely behind each other. This concept is shown and explored for PV systems in the report "Numerical simulations of wind loading on the floating photovoltaic systems" [9].

## 5.2   Flat plate

Due to limited resources and time, performing experiments on actual floating solar panels on indoor pools or in wind tunnels was instead done by simulating flat plate meshes for different wind speeds, $U_\infty$, and angle of attacks, $\alpha$. The flat plate will work as a standard for a solar panel in this thesis. It works well due to the fact that solar panels are generally flat, and only tilted to create the best efficiency. Therefore, a flat plate tilted by different $\alpha$ will resemble actual PV panels sufficiently enough.
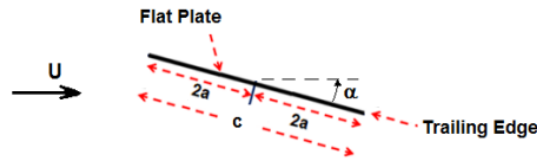


Figure 2: A illustration of a two-dimensional flat plate airfoil with chord length, c, angle of attack, $\alpha$ and velocity $U_\infty^2$ [4]

Geometrically speaking, the flat plate shown in 2 is the simplest form of an airfoil and has its aerodynamic pros and cons. The flat plate generates less lift, compared to that of an airfoil due to its non-curved surfaces resulting in smaller pressure differences between the upper and lower surface as the angle of attack, $\alpha$ increases.

The lift coefficient, $C_L$:

$$C_L = \frac{F_L}{\frac{1}{2} \cdot \rho \cdot U_\infty^2 \cdot A} \tag{2}$$

describes the lift force, $F_L$ being proportional to the airflow density, and surface area, and proportional to the square of the airflow speed and the lift coefficient. This is the same formula used in Apame to calculate the lift and drag coefficient. Where $F_L$ is replaced with $F_D$ for drag.

In practice, however, this is not the case by itself for the lift and drag. A book given out by Brennen, C [4] for fluid mechanics explains this is because of the turbulent airflow leaving the flat plate from the upper surface due to the flat plate's sharp leading and trailing edges. The sharp edges cause the airfoil to

experience a boundary-layer separation of the airflow and the flat plate surface, creating a wake on the upper surface which leads to much less lift than optimal as the $\alpha$ increases.

To avoid boundary layer separation, a specific circulation value is required. For a Joukowski airfoil solution, this circulation is calculated to be $\gamma$, calculated as:

$$\gamma = 4\pi r U_\infty sin(\alpha) \tag{3}$$

which is the only circulation value where the airflow leaves the flat plate smoothly [4]. In practice, at least for smaller angles of attack, this is done by rounding the leading edges to make the airflow stay more attached to the surface.
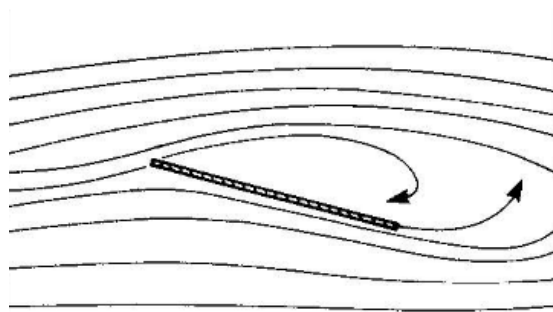


Figure 3: Flat plate stall point [11]

The maximum lift will appear right before the stall point as shown in 3, which is the highest angle of attack before boundary-layer separation between the upper surface of the flat plate and the airflow occurs, and the lift starts to significantly decrease afterward.

### 5.2.1 Pressure on a Flat plate

A general characteristic of a flat plate is illustrated here 2 shown to have a chord length of $c = 4a$ where the a represents the radius, R in a circular solution. By executing a Joukowski transformation of an already-known airflow of a circular cylinder, over to a flat plate, one is able to calculate the center of pressure that appears at $\frac{1}{4}$ chord length, c [1]. To prove this, a complicated calculation process is required, not befitting this thesis, and instead can be seen proved by Aerodynamics4students here; [1].

## 5.3 Aerodynamic forces

The lift force is defined to be perpendicular to that of the airflow. It is a product of differences in pressure created by a fluid flow on the top and bottom surfaces of an object. The drag force, on the other hand, is defined to be parallel to that of the airflow. The drag is a product of differences in pressure on the parts of the object facing towards and away from the airflow as well as viscous forces on the object's surface [10]. The lift, $C_L$ and drag coefficients, $C_D$:

$$C_D = \frac{F_D}{(\frac{1}{2} \cdot \rho \cdot U_\infty^2 \cdot A)} \tag{4}$$

are useful calculations in order to determine at which angle of attack the wind applies the most stress and work to the plates. The axial force is defined as parallel to the plate or foil, and the normal force is defined to be perpendicular to the plate or foil. Their relationship to the lift and drag forces, $\vec{F_L}$ and $\vec{F_D}$ respectively, can be explained through the equations:

$$F_L = N \cdot cos(\alpha) - A \cdot sin(\alpha) \tag{5}$$

and

$$F_D = N \cdot sin(\alpha) + A \cdot cos(\alpha) \tag{6}$$

where N is the normal force, A is the axial force, L is the lift force, D is the drag force, and $\alpha$ is the angle of attack. Both CFD and Apame produce results that need to be converted from axial and normal forces to lift and drag forces.

In figure 4 the aerodynamic forces working on a body in a fluid stream, lift $\vec{F_L}$ and drag $\vec{F_D}$, can be combined to produce the resultant force $\vec{F_R} = \vec{F_L} + \vec{F_D}$. The relationship between these forces is shown in figure 4.
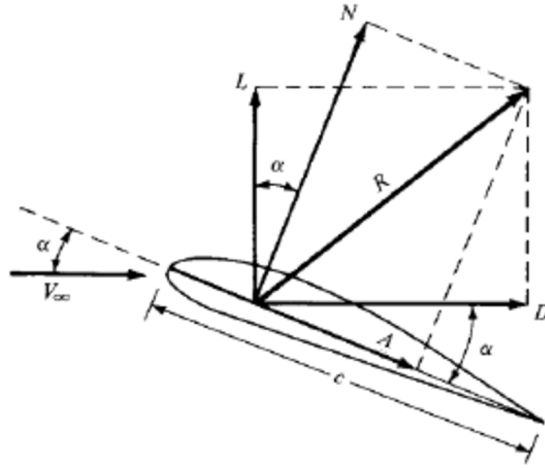
Figure 4: The relationship between lift ($F_L$), drag ($F_D$), and their resultant force ($F_R$), as well as normal ($F_N$) and axial ($F_A$) forces[17].

## 5.4 Analysis Tools

### 5.4.1 CFD analysis and simpleFoam

Computational Fluid Dynamics, CFD is a common designation given to powerful analysis and computational software for fluid dynamics. It makes it possible to analyze reality-based cases in a 3D scenario. Thus making it possible to change and perfect a design without making a physical prototype. The results are also relatively easy to interpret with programs like Paraview. Making it easier to see faults in a design. The biggest weakness of CFD is its huge power requirement, where more complicated scenarios require either a lot of time or a supercomputer, or both. [15].

The Program used for CFD analysis is BlueCFD, OpenFoam. OpenFoam is a C++ toolbox for the development of customized numerical solvers, one of them being CFD. The solver chosen in OpenFoam is simpleFoam which is a steady-state solver that uses the SIMPLE (Semi-Implicit Method for Pressure Linked Equations) method. simpleFoam is used in the airfoil and flat plate simulations in order to obtain the pressure field over the object and simulate reality-like wind cases. The simulated object consists of multiple nodes which the program interacts with to determine forces affecting the object. The wind simulated in simpleFoam will interact with the nodes on the object, creating a result file. Increasing the number of nodes in the object will result in more interactions and thus more, and longer calculations, but more precise results.

7

It is worth noting that increasing the number of nodes and interactions will require more process time and potentially a really powerful computer with enough processors to not shut down during the simulation.

### 5.4.2 3D Panel method

The panel method is a method used to approximate the forces working on an object. In this project, the program used for calculations is the open-source program Apame. The panel method is a method that can be used instead or supplementary to CFD. Especially in the R&D phase where more simplistic models are analyzed and created. It is less precise but has a lot shorter calculation time. Apame will give good results in cases where drag and friction forces can be ignored.

The panel method uses elemental flows. The object that is being analyzed is turned into multiple panels that each can be given an elemental flow. Together this can recreate the original shape of the object. In other words, the panels no longer exist but are instead flows that combined create the flow around the entire object. Thus, the weakness of the method with calculations of friction and drag, given that there no longer is a physical object. It is therefore no longer an interaction between the fluid flow and the object.

In terms of velocity calculation methods in Apame, there are three options; Nodal, First Order, and Second Order. The Nodal method utilizes first the doublet strengths in each node of the mesh before interpolating these values, then deriving them in order to obtain the velocity results. First Order is a linear interpolation of the nodes while Second Order is a quadratic interpolation. Both First Order and Second Order methods are more precise than the Nodal method and require more calculation time [18].

In addition to those three velocity calculation methods, Nodal, First-, and Second Order, one can also choose between Approximate and Accurate collocation point calculation. The Accurate method calculates the panel's center of weight, while the Approximate method averages the corner points' locations instead [18].

### 5.4.3 Mesh

The mesh is a data version of a 3D object which is then simulated in a program and has the goal of imitating the real-world object. For example, a PV panel will be imitated by a flat plate. The simulation will be better the closer the imitation is. The flat plate will for example not have the groves that are found in normal PV panels resulting in inaccuracies compared to physical

8

tests. The precision of a mesh has a direct correlation to the quality of the results. The more nodes, also called data points, there are in a mesh, the finer it is. The increased amount of nodes will result in more points for the simulation to interact with, thus giving a more precise result. The consequence is that it requires more calculation thus more time or a better computer. The opposite is true for a coarser mesh with fewer nodes. This will result in less precise calculations. It is therefore important to note that the quality of the mesh will have an impact on the results, giving a margin of error.

# 6 Methodology

## 6.1 Software Setup

During this project, the analysis programs blueCDF and Apame will be used to calculate the lift, drag, and forces working on the object. Additionally, the visualization program Paraview is used to gain more insight into how the wind forces affect the object for different AoAs. The CFD program gives a more accurate representation of real-world forces for different scenarios by using heavy computer processing, to get more accurate results. The panel method, Apame however, is a much more quick-based program using less processing power and is a good method to discover possible mistakes in the mesh coding before using the CFD method. The panel method will give less accurate results because of the way the calculations are done, with the benefit of a calculation time of minutes instead of days.

## 6.2 Blockmesh Creation and analysis

The Blockmeshes for the flat plate will be created by our supervisor at SIN-TEF, later a CFD analysis will be done of those meshes, furthermore simulated in Paraview. Due to the large amount of processing power required in order to do a CFD analysis, it was later determined it would be simplest if the 3D CFD cases were done at SINTEF. Then sent to us for post-processing and to compare the results against the panel method in Apame.

## 6.3 Validation

Validation is an important part of the project, where the group will run scenarios done in other reports to validate that the processes are done correctly and learn the programs. This will also give us a good indication of the differences in the calculation methods. There will be performed 3 different scenarios for validation. First, verification of CFD where the aerofoil NACA0012 is used. Then a verification in Apame where a NASA wing is analyzed, and finally, a flat plate in OpenFOAM and Apame.

### 6.3.1 CFD - NACA0012

The report used for reference for the NACA0012 airfoil is a previously written bachelor thesis by Åsmund Fossum from NTNU about noise production from airfoils[8]. The thesis includes multiple cases for the NACA0012 airfoil.

The values used for validation are more specifically the lift and drag values with a Reynolds number of $Re = 1.5 \cdot 10^6$. The Naca0012 CFD simulations were ran in a coarse and a fine mesh. The coarse mesh simulations were ran by the group, the supervisor did the simulations inn the fine mesh then Post-processing for both cases were done by the group.
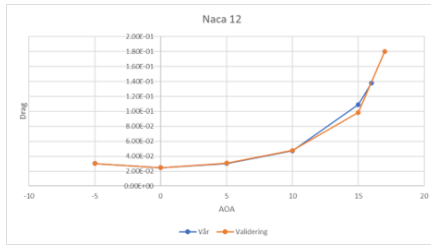


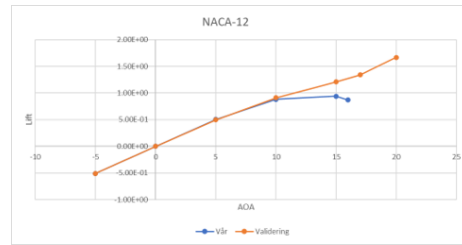Figure 5: NACA0012 $C_D$ for different AoA

Figure 6: NACA0012 $C_L$ for different AoA

The lift and drag coefficient results shown in figures 5 and 6 for NACA0012 match closely with the CFD results from Fossum's report [8]. A difference in results is noticeable after 10°, and after 17°the steady state could no longer be achieved. 16°is therefore the highest angle of attack that was computed for the NACA0012. The results were done with a relatively coarse mesh which also could have contributed to differences in results.
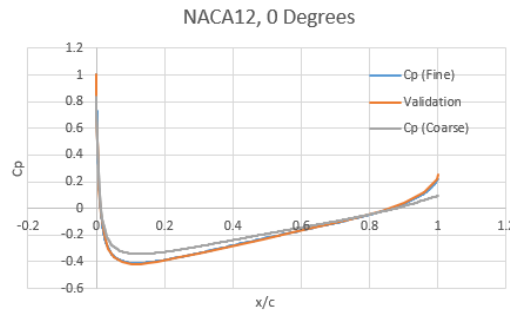


Figure 7: NACA0012 $C_P$ plotted against x/c at 0°
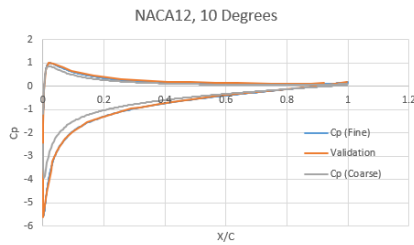
Figure 8: NACA0012 $C_P$ plotted against x/c at 10°
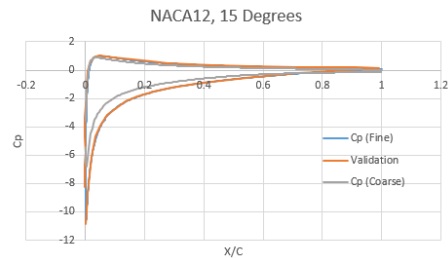


Figure 9: NACA0012 $C_P$ plotted against x/c at 15°

Figures 7, 8, and 9 show the pressure coefficient for NACA0012 plotted against normalized chord length $(X/C)$ for different angles of attack. The blue graph is done with a coarse mesh, the orange graph with a fine mesh, and the gray graph is the result of the validation report from NASA.

The calculated pressure coefficient with a fine mesh matches the validation graph and report exactly, shown in figure 7, 8, and 9. The coarse mesh has fewer mesh elements than the fine mesh. Therefore the calculated $C_P$ for the coarse mesh results are not as precise as the fine mesh results and subsequently stray more from the validation results. This is especially clear in areas where the $C_P$ value has drastic changes. For example at the front end of the wing around $X/C$ 0. The same coarse mesh is used for the lift and drag calculations. The mesh could have played a part in the difference in results for lift and drag with the validation report. The results show that the approach matches well with previous reports and that the CFD approach used in this report works for NACA0012 and the impact a coarser mesh will have on the final results.

### 6.3.2   Apame - NASA wing

With guidance from our supervisor, in order to obtain more quick-paced results of the forces working on the flat plate - the panel method in Apame was used. This method gives quicker results and is only estimated results, and not exact. The intent is that the panel method gives a good indication of potential mistakes in the mesh or other factors in the design, which would affect the results. Making it possible to improve a design without using CFD, thus saving time. To learn the program a tutorial by Etienne Vandame [18] was followed. It shows the steps done in the NASA wing validation process, all the steps was done by the group followed by processing the results.
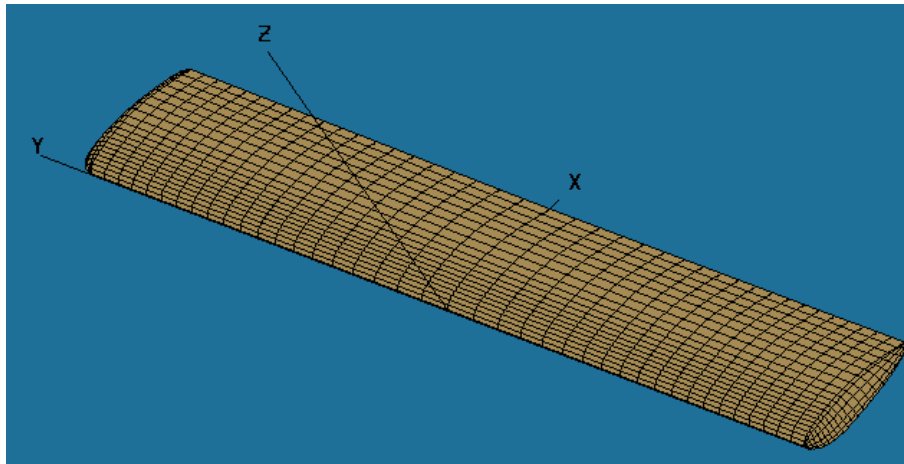
Figure 10: Wing validation done in Apame

To begin with, a validation of a plane wing 10 was done in Apame to obtain its lift and drag forces by adjusting the angle of attack from 0 to 16°. Giving it a Wingspan of 4.013 m, a Mean Aerodynamic Chord (MAC) of 0.447 m, and a Surface area of 1.795 $m^2$. All these values are gathered from the official NASA report [13].
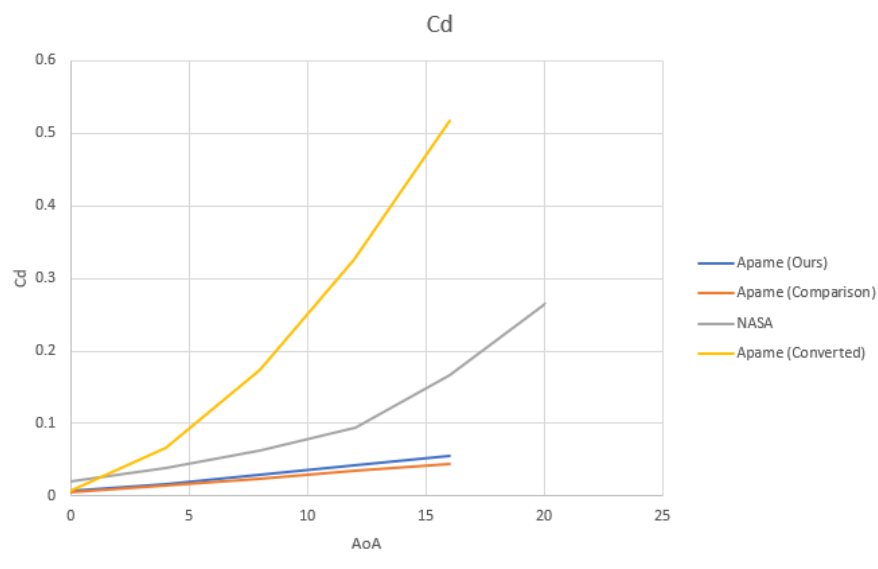


Figure 11: Drag forces, $C_d$ working on a wing

Figure 11 shows the drag results working on the plane wing, 10 from 0°to 16°. The study includes an original result, as well as a NASA validation and an Apame validation. Figure 11 shows that the blue and orange lines for Apame results are fairly similar in terms of the value of drag force based on the angle of attack with the NASA results, the grey line, having greater drag force at the same AoA. However, after an increase of the angle of attack up to 12°, the NASA validation of the drag force starts to incline drastically from 0.095 to 0.167 at 16°, and to 0.265 at 20°having almost a linearly increase. The Apame validation as well as the Apame results had a drag of 0.035 and 0.042 respectively at 12°and 0.044 and 0.055 at 16°. The yellow line shows the usage of radians instead of angles in the drag calculations and shows a much greater drag increase compared to the blue and orange lines having also a much higher drag than the official NASA report as well.
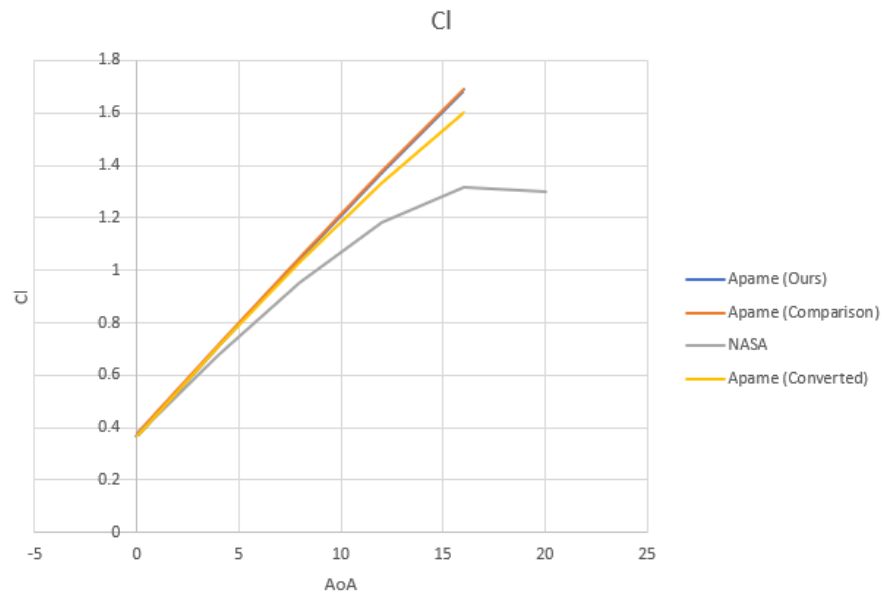


Figure 12: Lift forces, $C_l$ working on a wing

Figure 12 shows the lift results working on the plane wing, 10 from 0°to 16°. Just like the figure for drag above, this illustration includes an original result, an Apame validation, and a NASA validation. The NASA validation is measured from 0°to 20°. In figure 12 the lift is shown to be just shy of an exact match for the blue and orange lines all the way through, and the lift values converted using 5 (yellow line) also gives very similar results. Whereas the NASA report shows a lower lift result for the same angles of attack, having a steady increase and reaching its maximum lift at 16°before slowly decreasing until 20°.

### 6.3.3 Apame - Flat plate

Going from an airfoil simulation, a flat plate validation in Apame was done by the group following the study, [5] for wind loads on FPV systems using a flat plate illustrated in 14. The research study used a single commercial module PV panel with a width of 0.6 m and length of 1.2 m in their experiment setup, giving it a wing span surface area in Apame of 0.72 $m^2$. Being 60% scaled and having a wind velocity of 14.5 $m/s$ the study was performed in a wind tunnel for 0-90°angles of attack, AoA, and 0-165°sideslip angles (YAW), and obtaining the lift results shown in 13.
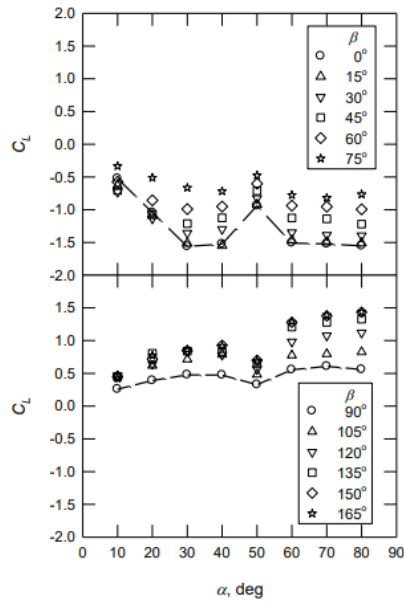


Figure 13: Research study for lift load working on the FPV system [5]
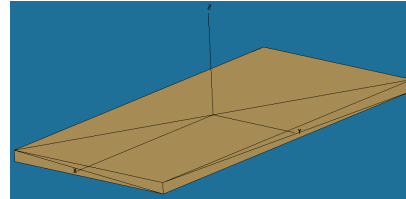


Figure 14: Apame validation of the research study using a flat plate

Figure 14 shows a 0.6 m wide and 1.2 m long flat plate in Apame which was used to validate the results done by [5] and to obtain the results 13. The flat plate 14 shown only contains 8 nodes and needed to be refined to obtain promising results. Firstly, two tests were done using a refined mesh with 800 and 3000 nodes respectively, and different calculation methods to determine the best method. Afterward, two tests were done with the best method found using a variety of different refined meshes to determine the best mesh, at 0 YAW. Lastly, two studies were done with the determined mesh and calculation method for 0 and 45 YAW, to obtain the most accurate lift forces and to show changes in lift for an increase in YAW angle.

15
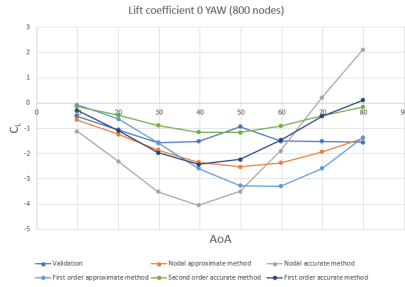
Figure 15: Apame validation with 800 nodes flat plate with different methods
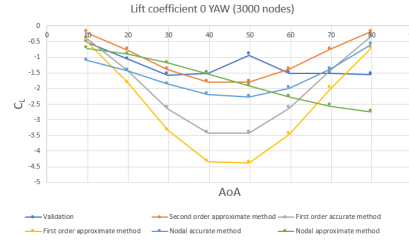


Figure 16: Apame validation with 3000 nodes flat plate with different methods

Figure 15 shows the flat plate lift results for 800 nodes from 0-90°AoA and 0°YAW using different calculation methods in Apame. Likewise, figure 16 shows the flat plate of 3000 nodes with 0-90°AoA and 0°YAW for multiple methods. Based on these results, Nodal Approximate Method and First Order Accurate Method were seen as the most accurate methods for the validation. The wing surface area needed to be increased to achieve reasonable values for all methods. The Nodal method required the least increase in area. The increased unit was $10^3$ for the nodal method and $10^4$ for First Order and Second Order Approximate. For the Second Order Accurate method, the increase could be as high as $10^7$ if a realistic result were desired depending on the number of nodes in the mesh.
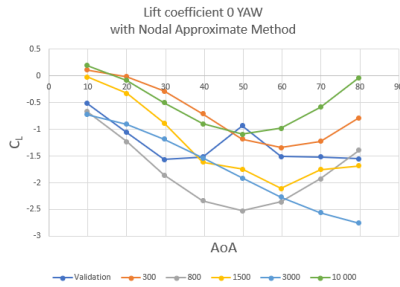


Figure 17: Apame validation using Nodal Approximate Method with changing mesh
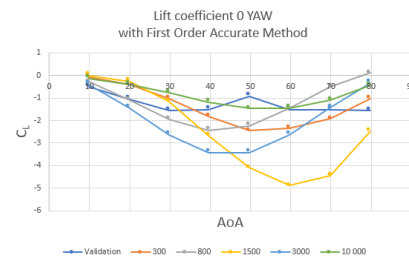


Figure 18: Apame validation using First Order Accurate Method with changing mesh

Figure 17 shows the flat plate lift results for different meshes ranging from 300 to 10 000 nodes, 0-90°AoA and 0°YAW using the Nodal Approximate Method. Likewise, figure 18 shows the flat plate from 300 to 10 000 nodes with 0-90°AoA and 0°YAW using the First Order Accurate Method. Based on these results, the 800-node mesh and 10 000-node mesh proved to be the

most accurate for both cases. Regardless, the 800-node mesh performed more accurately than the 10 000 mesh but chose to continue with the 10 000 mesh based on the fact that the actual FPV system done in this study will naturally include many more nodes than 800 and more close to the 10 000 mesh.
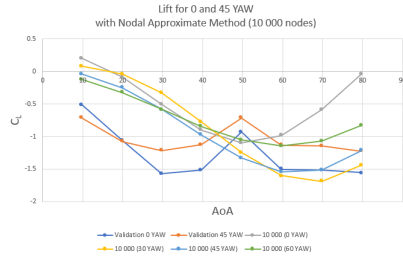


Figure 19: Apame validation for 0 and 45 YAW using Nodal Approximate Method for the 10 000 node mesh
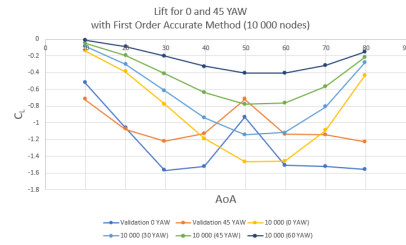


Figure 20: Apame validation for 0 and 45 YAW using First Order Accurate Method for the 10 000 node mesh

Figure 19 shows lift results for a 10 000 node mesh using the Nodal Approximate Method in Apame for 0, 30, 45, and 60 YAW angles to show the change in lift based on different YAW angles. Likewise, figure 20 shows the lift results for the same mesh and YAW angles, but using the First Order Accurate Method. Even though the 800-node mesh looked promising for 0 YAW for both Nodal Approximate and First Order Accurate methods, after performing calculations for 30, 45, and 60 YAW, the 800-node mesh proved to be very inaccurate and not really optimal for the validation.

For cases done in this thesis, the stalling point for the NACA0012 and NASA wing validations proved to be at 16°AoA with the NACA0012 simulated with CFD and the NASA wing in Apame. For the flat plate in Apame, the stalling point for the most part occurred at 50°AoA, with sometimes occurring at 40°.
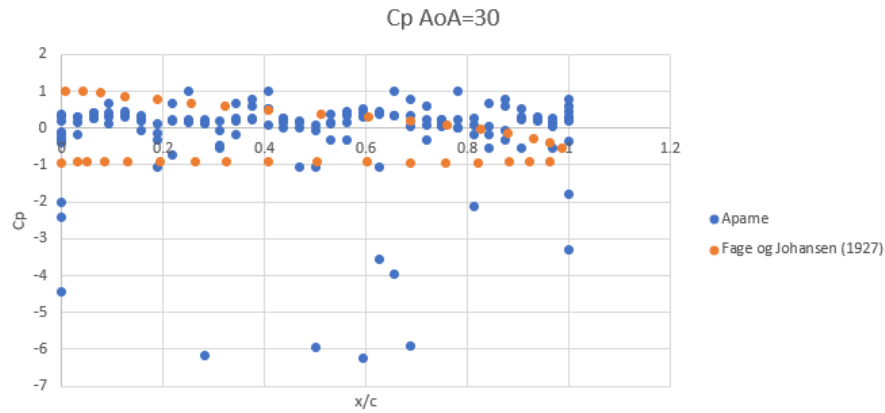
Figure 21: Pressure coefficient on a flat plate at $\alpha = 30°$

The Pressure coefficient extracted from Apame is of little use, It does not work to sort the lines in programs like Paraview. The plot over is done in Paraview with sorted lines, but Paraview does not manage to sort the lines correctly. Figure 21 shows that there is a substantial amount of outlier points in addition to not matching with the validation report. The problem consists of all angles of attack. These problems combined show that extracting CP for Apame has little purpose and will therefore not be done later in the report.
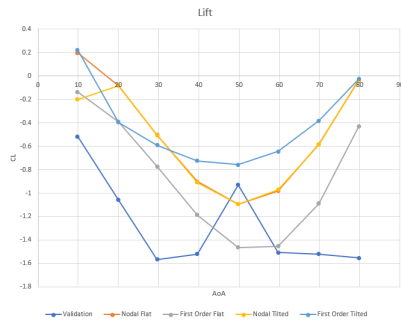


Figure 22: Apame flat plate validation with tilted and non-tilted meshes
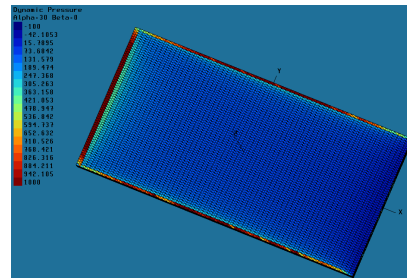


Figure 23: Cp plot for the flat plate validation

The graph above is done with manual tilt and tilt done in Apame. Manual tilt means rotating the mesh in mesh-lab and then making an individual mesh for each angle of attack. The tilted meshes also have the normals straightened so that they face perpendicular to the surface. As shown in the graph above manual rotation have a direct impact on the results. The pressure plot has a

18

lower pressure coefficient at the top of the leading edge then slowly increases to the trailing edge. The opposite is the case of the underside of the plate. With the leading edge having the highest pressure and the low pressure on the trailing edge.

### 6.3.4 CFD Flat plate

The report used for validation is [16]. It is a report that looks at lift and pressure coefficients for different angles of attack. The mesh used in the report has an aspect ratio of 5 with a wind speed of 10 $m/s$. It is important to note that there are some geometric differences. The plate used in the validation report is curved, making it more like an airfoil, but the one used in this report is a normal flat plate. The figures 24, 25, and 26, below show Cp for different angles of attack. The Cp value represented as a blue line in the figures below was done at SINTEF by the group's supervisor using the CFD method and the figures show the post-processing of the CFD results compared to other similar reports done by the group.
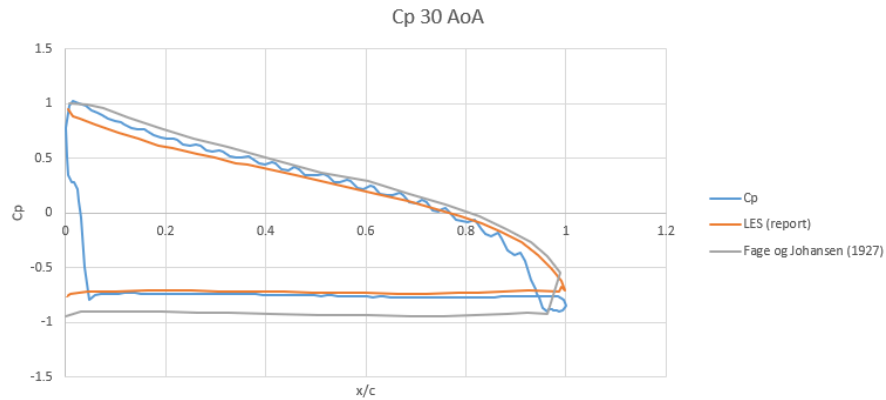


Figure 24: Pressure coefficient on a flat plate at $\alpha = 30°$

Figures 24, 25, and 26 show that the top of the plate matches well with the validation results for all the graphs, but quite different for the underside. The discrepancy is caused by the difference in curvature for the geometry.
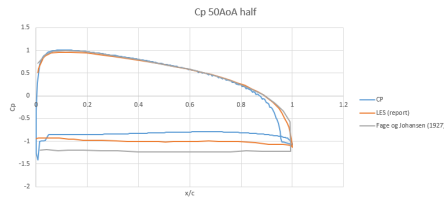
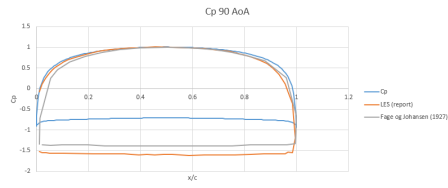Figure 25: Pressure coefficient on a
flat plate at $\alpha = 50°$

Figure 26: Pressure coefficient on a
flat plate at $\alpha = 90°$

The CFD validation results show that the approach is consistent and gives
good results, the discrepancy can largely be contributed to known factors that
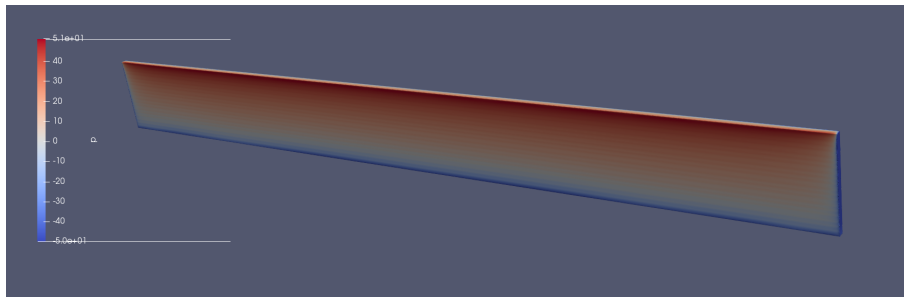are further shown by the pressure plots' similarities with Apame.



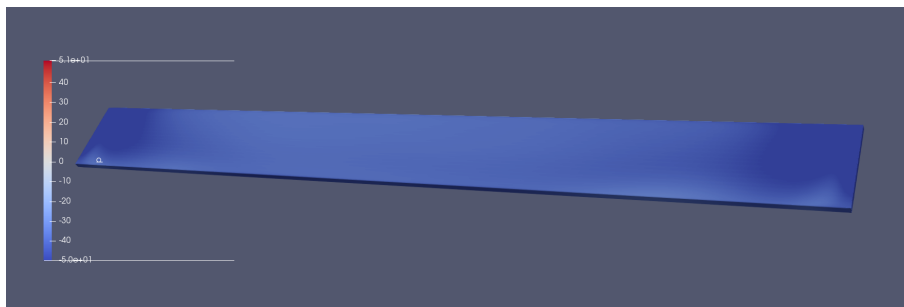Figure 27: Pressure plot from $\alpha = 30°$ plates under side displayed in Par-
aview



Figure 28: Pressure plot of a $\alpha = 30°$ plates top side displayed in Paraview

The Pressure on the underside starts at high pressure by the leading edge and
then slowly decreases until it has low pressure at the leading edge. The pres-
sure distribution is quite different for the overside, with two low-pressure re-
gions on both sides of the plate and a slightly higher pressure in the middle.

20

The trend of sinking or increasing toward neutral pressure can be seen at the sides, but it is much less pronounced than on the underside.

## 6.4   FPV

This study will focus on the rare mean wind speeds occurring each 50 and 100 years time period in order to be prepared for worst-case scenarios. The 4x4 FPV system consists of 16 panels in total with a total of 64 bridges connecting the panels, with 32 facing wind in the x-direction and 32 facing the y-direction. Tests will be performed on a 4x4 FPV system using wind velocities of 10, 15, 20, and 25 $m/s$. The reference area for the 4x4 FPV system is estimated to be 60.4 $m^2$, with each panel being 1.9 m in both length and width and each bridge being 0.19 m in length and 0.11 in width. These tests will include a CFD simulation done in blueCFD and a 3D panel method, done in Apame.

### 6.4.1   Apame

For the Apame simulation of the PV network, multiple meshes were used and compared. As a standard, the 4x4 FPV system mesh consists of 640 nodes but is further refined to have 4000 nodes. First, a mesh at 0°was used with the built-in tilt function in Apame with 10°steps between 0°-40°. Then the mesh was tilted with 5°steps in meshlab, and results were produced for each mesh from 0°-40°. Both mesh types were simulated using the two main calculation methods, First Order Accurate and Nodal Approximate. These results were then plotted in Excel together with the CFD results for the PV system.

### 6.4.2   CFD

The CFD will have some differences in setup compared to Apame. CFD will only be run at an angle of attack from 0°-15°and a wind speed of $10m/s$. The mesh will also have some differences, where the Apame mesh is flat and smooth the CFD mesh will have a staircase structure for all the angles of attack higher than 0. This is done because of the CFD programs used. If a completely smooth mesh were desired the node count would have to increase, thus making the run time longer. An example of the staircase structure is shown in attachment A.138.

# 7 Results

## 7.1 FPV system

The PV network simulated by the panel method and CFD is constructed with multiple flat plates connected with thin bridges as illustrated in figure 29. The FPV system is a 4 by 4 layout making it a total of 16 solar panels. The simulated wind velocity varies between 10 $m/s$ to 25 $m/s$ with increments of 5 $m/s$, making it a total of 4 different wind speeds. Worth mentioning that even though the wind speed changes from 15 to 25 $m/s$, based on the lift formula 2, the results in the Apame calculation are the same or too small that it doesn't show in the results. The CFD simulations were done by the group's supervisor at SINTEF, and the group did the post-processing of the CFD results as well as ran and post-processed the Apame simulations.
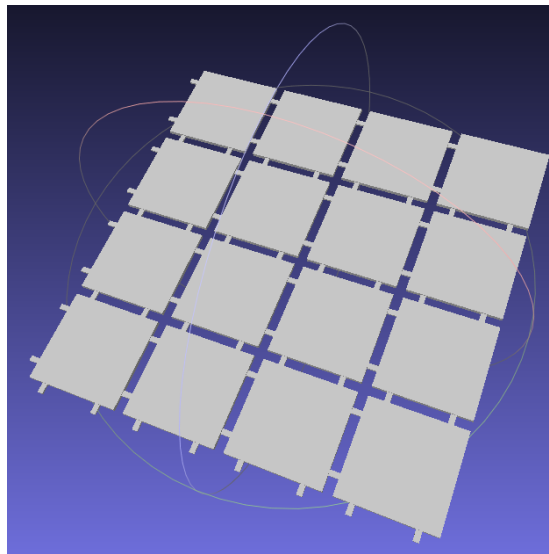


Figure 29: Illustration of the 4x4 FPV system used in Apame calculations (Picture taken from meshlab).

The calculation methods used are Nodal Approximate and First Order Accurate which are based on the results obtained from the Flat plate validation done prior in section 5.3.3 where those methods came out as the best across all meshes.

### 7.1.1 Lift and Drag

Figure 30 and 31 show the drag and lift coefficient forces working on the 4x4 FPV system. Figures 30 and 31 include three different comparisons of lift and drag. The yellow and dark-green lines in figure 30 a flat FPV system (0°AoA) which entails a 0-40°AoA calculation is manually done in Apame. In figure 31 the yellow and grey lines represent the flat FPV system. The light-green and blue line in figure 30 shows a "Tilted" simulation version in Apame entailing an FPV system mesh that is tilted from 0-40°AoA in the mesh prior to the simulation, and only needed to use 0°AoA in Apame. The "Tilted" line in figure 31 is the orange and dark-blue line. Lastly, the dark-blue line in figure 30 shows a CFD simulation version done in blueCFD for 0-15°AoA. The CFD line in figure 31 is the light-blue line.

The calculations included AoA ranging from 0-40°in Apame, with 0 YAW, and from 0-15°in blueCFD. A surface area of 60.4 $m^2$, and wind velocity from 10 $m/s$ to 25 $m/s$, with 10 $m/s$ in blueCFD, using the Nodal Approximate and First Order Accurate methods in Apame. Based on results obtained from the flat plate validation in section 5.3.3 the First Order method gives roughly 10 times greater lift and drag coefficient results compared to the Nodal method, believed to be because of a change in unit done by the program. In order to get similar results as the Nodal Approximate method, the surface area was increased to 604 $m^2$ for the First Order Accurate method, This matches with results in validation where it was discovered that first-order needs 10 times the area of nodal.
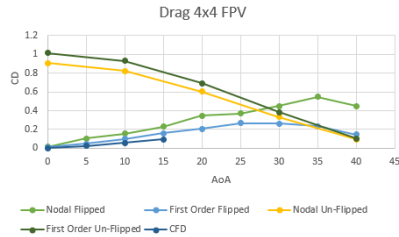


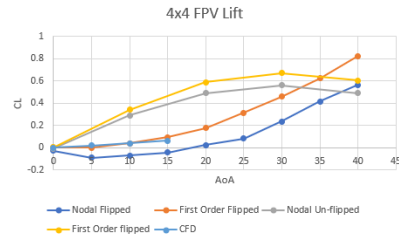Figure 30: Drag coefficient of a 4x4 FPV system in Apame



Figure 31: Lift coefficient of a 4x4 FPV system in Apame

Figure 30 and 31 show the drag and lift coefficients of the 4x4 FPV for the three comparisons. Figure 30 shows that the drag results for the flat FPV start off at their maximum point at 0°AoA and steadily decrease in value till 40°AoA. On the other hand, the tilted drag results in figure 30 is shown to be very aligned with the CFD drag results, which are much more concrete results compared to that of Apame, all the way up to 15°AoA. The tilted drag results continue to rise after 15°AoA till 25°AoA for the First Order

method and then start to sink in value until it reaches 40°AoA, while the Nodal method doesn't start declining in value before it reaches 35°AoA. Out of the Nodal and First Order methods for the drag results in figure 30, the CFD results are shown to be more matched with the First Order method from 0-15°AoA.

Figure 31 shows that the CFD results for the lift very much match the First Order method for the tilted version of the simulation. The lift results for the flat FPV in figure 31 had a more aggressive incline compared to the tilted version and CFD lift results, and it reached a stall point at 30°AoA. The tilted lift results in figure 31 showed a more curved incline in the beginning like the CFD results but don't show a reached stall point as of 0-40°AoA.

The system was also simulated in CFD for an angle of attack from 0 to 15 degrees. There are some differences from the simulations in Apame. First, the wind speed in CFD was $10m/s$. Second, the meshes were drastically different from all angles except 0 degrees. The meshes above 0 degrees have a staircase-like structure. This is observable in figure 33 or in attachment A.1 38 for a more clear picture. The shape will have a noticeable impact on the forces impacting the FPV system.
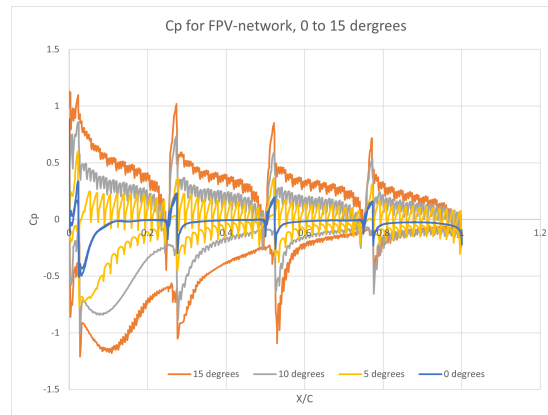
### 7.1.2  Pressure distrubution



Figure 32: Graph showing Cp in regards to relative chord-length

Figure 32 show the pressure coefficient, $C_p$ for the simulated FPV system for all simulated angles of attack. The $C_p$ values were extracted over the bridge connecting the panels. The "bridges" can be observed in the picture 33. Each graph can be divided into 4 parts each corresponding to a PV panel. The

24

shape is consistent through each sector for the given angle of attack but decreases in value the further away the panel is from the leading edge. All the little bumps shown in each section correspond to the amount of "stair steps" in the given mesh. There are for example more steps for the 15 degrees than the 5 degrees, resulting in fewer bumps in each part for the 5 degrees. The graph also shows a substantial increase in $C_p$ for each step up in the angle of attack. The max $C_p$ value for each panel is at the leading edge, where it slowly decreases until it hits the next leading edge where it increases to a value a bit lower than the previous leading edge.
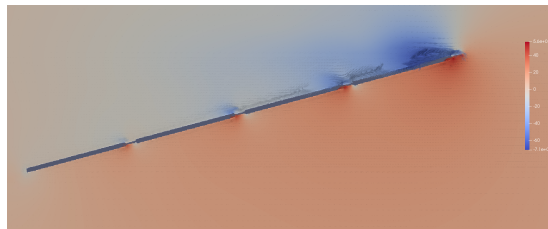


Figure 33: Illustration of pressure and wind in 4x4 FPV with AOA 15 degrees

Figure 33 illustrates the pressure and wind forces along the FPV system with an AoA of 15°. The illustration is over the bridges connecting the panels, for an illustration without the bridge check out attachment A.239. Note that the leading edge is on the opposite side of the $C_p$ graph. It is clearly illustrated that the leading panel edge is affected by the most pressure. Then it slowly decreases along the panels until the wake is almost non-existing. This matches well with the $C_p$ graph for 4x4. The separation of the boundary layer mentioned in section 4.2 about the flat plate is also clearly shown on each panel.
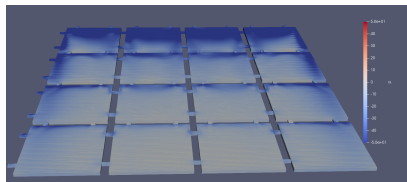


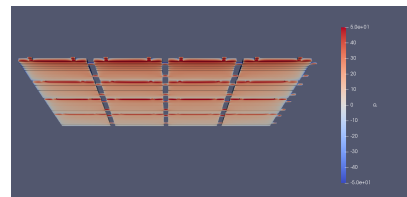Figure 34: Paraview plot of the forces on 4x4 FPV from above in CFD



Figure 35: Paraview plot of the forces on 4x4 FPV from below in CFD

A pressure plot is a different way of showing the forces on the FPV system. Both figure 34 and 35 show pressure for an AoA of 15°. The pressure is the highest at the leading edge of each panel and then slowly reduces towards the

trailing edge. For the top portion of the system, there is high negative pressure, and at the underside, there is positive pressure, displayed in blue and red respectively. Then the process restarts for each panel having a slightly reduced peak shown in graph 32. It is not shown clearly in the pictures above, but the pressure on the bridges going perpendicular to the wind is consistently higher than the midsection of the plates they connect to. The bridges parallel with the wind have about the same negative pressure as the center of the panel for the top side. The pressure on the underside of said bridge has a drastic pressure differential across the bridge. Where the back end of the bridge experience the same pressure as the leading edge it is connected to and the front has the pressure of the trailing edge it is connected with. For a more clear picture look at attachment A.340.
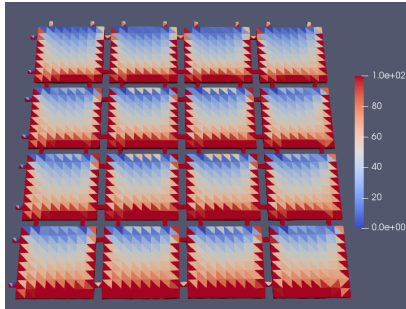


Figure 36: Pressure plot displayed in Paraview for the 4x4 PV system from above in Apame
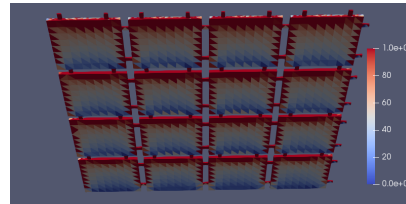


Figure 37: Pressure plot displayed in Paraview for the 4x4 PV system from below in Apame

The pressure plot from Apame is from an AoA of 30 degrees and a wind speed of $10m/s$. The pressure distribution is the same for the underside at the top of the system, but each side mirrors the other. The pressure displayed ranges from 2 to -6. For the underside, the pressure is at its peak on the leading edge and then slowly decreases to the minimal value at the trailing edge. That is the opposite of what happens at the top side. The sides of the panels have slightly lower pressure than the center. The sheltering effect is not present in the Apame pressure plots. Shown by the fact that the pressure does not decrease from the first panel to the last, but rather has largely the same pressure distribution and values. The bridges running perpendicular to the wind have the same pressure as the center of the panels. The bridges diagonal with the wind have a lower pressure than the center of the panels. The bridges parallel to the wind start with low pressure at the trailing edge of the panel, then the pressure increases across the bridge until it meets the trailing edge of the following panel for the underside and opposite for the top side, shown in attachment A.4-5 41. The pressure distribution will be the exact same for different wind speeds. That matches with the fact that Lift and drag are the

same regardless of the wind speed. The pressure increases with increased wind speed. The pressure distribution at $25m/s$ can be observed in attachment A.6-7 43. It clearly shows the same distribution, but much higher pressure from the increased wind lowed.

# 8 Discussion

## 8.1 FPV system

### 8.1.1 Lift and Drag

The graphs 31 and 30 in section 6.1.1 show that the lift and drag match well with the calculation done in CFD, but this is cotangent on certain steps being followed. It is clearly shown that a manually tilted mesh gives vastly different results compared to an Apame tilted mesh. The First Order method gives much better results than the Nodal, especially for the tilted mesh where the Nodal lift coefficient is largely useless for the first lift values. The biggest difference between a tilted and a flat simulation is in the drag. Where the drag for the system tilted in Apame starts at its max value and then slowly decreases with higher angles of attack. That is not realistic and is the exact opposite of what really happens. It is therefore important to flip the mesh manually. The curvature of lift and drag matches well with the CFD results, especially for the First Order method. The Wing area used for calculation in First Order was 10 times that of the real wing area($60.4m^2$), used in nodal.

### 8.1.2 Pressure distribution

The $C_p$ graph 32 clearly shows a sheltering effect that reduces the pressure on the panel the more panels there are between the panel and the origin of the wind, much like the sheltering effect described in report [9] and in section 4.1 Wind characteristics. The sheltering effect is shown in all plots and figures from the CFD analysis. Apame does not show this effect. Plate-method relies on the flow following the mesh or the edge of the simulated object, and can therefore not simulate wakes. These wakes are what cause a sheltering effect, thus Apame can not and will not simulate the effect. Nonetheless, the pressure plot in Apame has a lot of similarities with the CFD plots. The pressure distribution across a panel is very similar if the value is not taken into account. For example, both have the lowest pressure on top of the leading edge where it then slowly increases towards the trailing edge. Then the opposite is on the underside where to pressure is the highest on the leading edge and then slowly decreases towards the trailing edge. Both have relatively neutral pressure values on the bridges perpendicular to the wind and high on the bridges parallel to the wind, with a drastic pressure differential across the bridges. Therefore both methods show the same point of contention for the structural integrity of the FPV system, that being the bridges and the edges of the panels. Apame also shows the increased pressure caused by increased wind loads. where the pressure increased more than 10 times with a wind speed increase from 10 to $25m/s$. The values calculated in Apame have about

28

the same range as CFD of about 100 units, but Apame has much higher pressure than CFD. CFD has a pressure range from 50 to -50Pa and Apame from 100 to -13Pa. The positive pressure is much higher in Apame and more evenly spread out in CFD. this is most lightly caused by Apame's inability to simulate wakes. Since most of the negative pressure comes from the wake following the leading edge.

On the ocean, the wind won't have a set direction, but will rather come from all directions depending on the time. If we create a situation with a much bigger system where wind can come from all directions. CFD analysis would clearly show that the pressure on the solar panels on the edges would be substantially higher compared to the panels in the center, thus showing that the bridges and the outer panel edges require less mechanical strength in the center, than the edges of the FPV system. Apame would not show the same, it would show largely the same pressure distribution across the system but would lack the sheltering effect and the high negative pressure. It would therefore show that the same parts of the panels are under pressure but would not show the decreases in mechanical strength needed for the panels closer to the center. Apame would in other words show that the whole system needs the same structural integrity, and CFD would show that the structural integrity needed in the center could be reduced.

## 8.2   Calculation methods

### 8.2.1   Apame

Apame was meant to be a counter to the time-consuming CFD analysis and there was a known problem with it being less precise. That problem has been further shown through the whole validation process and lastly in the results. The biggest problem has been finding consistency in the program. What works for one mesh is the exact opposite of what gives good results in a different mesh. This is for example shown in figures 18 where the First Order method is good for an 800 nods mesh but does not work well for the 2500 mesh. The inconsistency makes it hard to work with.

The next inconsistency is getting the right unit or value. Using the correct wing area has been challenging throughout the whole process, because the required wing area change depending on the method and mesh. There has with time been shown general rules but the program seems to brake those rules quite often. For example the area for the flat plate needed to be 1000 times larger for the Nodal method for most meshes to get answers in the correct value range. That was the case for close to all meshes no matter how fine the mesh was. But for a mesh with about 1500 nodes, the actual wing area of $0.72m^2$ instead of $720m^2$ gave the correct value. If you took a mesh with more

nodes than 1500 again, an area of 0.72 $m^2$ would be too insufficient in terms of lit and drag results again. This tendency was even worse for the Second Order method where the area needed seemed to increase with the refinement of the mesh.

The last inconsistency is the angle of attack. You can change the angle of attack in Apame. That way you can run the calculations faster and are able to skip the phase of making a new mesh or turning the mesh. But the fact remains that each method gives different results. This is for example shown in figure 31 and 30. This points to it being some sort of conversion error in Apame.

When all of the inconsistencies are known, Apame did what it was meant to do. The validation process shows that the results from Apame are off or just wrong for the higher angles of attack. This can be contributed to that the panel method relies on the flow following the mesh which does not happen in reality. Therefore when that is simulated through all the angles of attack it gives values that are wrong. In other words, Apame is not a method that should be used on higher angles of attack.

Apame requires either another method as validation or a thorough understanding of the subject. As mentioned earlier choosing the correct wing surface area is hard, it depends on a lot of factors. This can be countered by either having values from other calculations to compare with or having a good understanding of the object that is being analyzed. Thus knowing roughly what lift values should be expected. The pressure plots are also good for visualization of how the forces affect the object but the actual $C_p$ values are largely useless.

### 8.2.2 CFD

The validation process showed that the CFD gave consistent, good results that matches well with results in other reports. The main problem still remains, being the long calculation time, but the results have been shown to be consistent and good. High angles of attack are also a problem for CFD. Because high angles of attack increase the calculation difficulty with bigger wakes and other phenomenons thus increasing the calculation time and power needed for good results. This requirement is further highlighted by the fact that there was not enough time to run cases at other PV layouts, wind speeds, or angles of attack.

### 8.2.3   CFD compared to Apame

CFD has through the whole report shown to give better results, but there have also been much less cases done. Through learning Apame there have been hundreds of scenarios done with minor changes each time. For CFD, there's only been done a few cases. Some of the differences can be contributed to our focus switch from CFD to Apame when the cases started requiring a supercomputer with enough processing power. The results in Apame have always been quite off. They have gotten more realistic over time, but still vary quite a bit from the CFD results. The pressure plots in Apame match well with CFD. Apame could thus for example be used to check which parts of the FPV systems need sheltering, but not to analyze if the sheltering works. It has also become apparent how much more efficient Apame is. There has been multiple iteration and changes done for each result in Apame. Where there have been much fewer iterations and cases for CFD. That was because the time required for CFD became too long, especially for the FPV systems. Therefore, there was only time for analyzation of one FPV system at one speed.

# 9 Conclusion

It is clearly shown in both Apame and CFD that the lift and drag steadily increase with AoA. Both show that the bridges and the leading edges of the panels experience the most pressure. The similarities in pressure distribution are especially good if all steps are followed. If done correctly the pressure plots in Apame are good, given that the known limitations of the program are taken into account. The pressure plot in Apame could for example be used to understand which part of the system needs sheltering. Then CFD could be used to understand if the sheltering works. That would halve the number of iterations in CFD, thus saving a substantial amount of time. Apame is still too inaccurate and inconsistent for them to be used in more complicated calculations. First Order has proved to be the better of the two chosen methods in Apame for results but Nodal is useful to get an indication of what wing area needs to be used, given its consistency throughout all meshes.

Apame has proven to be a viable edition if the program is used correctly. That means using the First Order method for the best results and nodal for an indication of the simulated wing area. The meshes need to be manually tilted, not doing so can cause drastically different pressure plots and lift and drag values. Cases that rely on wakes and high negative pressure should not be simulated in Apame for anything else than an indication of where the pressure centers and distribution are. Anything out of that scope pushes the boundaries of Apames and the panel methods' capabilities. Together, CFD and the panel method can work to complement each other and create a more efficient and less time-consuming R&d process.

# References

[1]  Aerodynamics4students. *Lift and moment coefficients of a flat plate airfoil*. Last accessed 29 March 2023. URL: http://www.aerodynamics4students.com/subsonic-aerofoil-and-wing-theory/flat-plate-lift.php.

[2]  M Barnard. *Floating solar on pumped hydro*. Last accessed 18 April 2023. 2019. URL: https://cleantechnica.com/2019/12/26/floating-solar-on-pumped-hydro-part-2-better-efficiency-but-more-challenging-engineering/.

[3]  Tom Benson. *Boundary Layer*. (accessed: 22.03.2023). URL: https://www.grc.nasa.gov/www/k-12/BGP/boundlay.html.

[4]  Caltech. *The Flat Plate Airfoil*. Last accessed 28 March 2023. URL: http://brennen.caltech.edu/fluidbook/externalflows/lift/flatplateairfoil.pdf.

[5]  Ping-Han. Chung et al. *Wind Loads on Offshore Floating Photovoltaic Panels*. Last accessed 5 May 2023. 2018. URL: https://www.researchgate.net/publication/339301748_Wind_Loads_on_Offshore_Floating_Photovoltaic_Panels.

[6]  J.P. Coelingh, A.J.M. van Wjik, and A.A.M. Holtslag. *Analysis of wind speed observations on the North Sea coast*. Last accessed 26 April 2023. 1998. URL: https://www.sciencedirect.com/science/article/abs/pii/S0167610597002857.

[7]  DNV. *ENVIRONMENTAL CONDITIONS AND ENVIRONMENTAL LOADS*. Last accessed 22 March 2023. 2010. URL: https://home.hvl.no/ansatte/tct/FTP/H202120Marineteknisk20Analyse/Regelverk20og20standarder/DnV_documents/RP-C205.pdf.

[8]  Å. Fossum. *Assessment of Noise Production from Airfoils for Wind Turbines*. 2022.

[9]  L. Guy-Han et al. *Numerical simulations of wind loading on the floating photovoltaic systems*. Last accessed 26 April 2023. 2021. URL: https://link.springer.com/article/10.1007/s12650-020-00725-z.

[10]  Anthony Rogers James Manwell Jon McGowan. *Wind energy explained: theory, design and application*. 2009.

[11]  Kaiming. *Stall and flow separation*. Last accessed 25 April 2023. 2019. URL: https://www.cnblogs.com/code-saturne/p/10712791.html.

[12]  meteoblue. *Simulated historical climate  weather data for North Sea*. Last accessed 29 April 2023. 2023. URL: https://www.meteoblue.com/en/weather/historyclimate/climatemodelled/north-sea_united-states_5129210.

[13]  NASA. *Wing-body aerodynamic characteristics*. 2023, (Visit 12.04.23). URL: http://www.vandame.eu/tutorials/NASA-TN-D-8524.pdf.

[14]   Pilotfriend. *The boundary layer*. Last accessed 7 May 2023. URL: `http://www.pilotfriend.com/training/flight_training/aero/boundary.htm`.

[15]   Rambøll. *COMPUTATIONAL FLUID DYNAMICS (CFD)*. 2023, (Visit 18.04.23). URL: `https://no.ramboll.com/tjenester/bygg/vvs/cfd`.

[16]   M. Shademan and A. Naghib-Lahouti. *Effects of aspect ratio and inclination angle on aerodynamic loads of a flat plate*. Last accessed 2 May 2023. 2020. URL: `https://aia.springeropen.com/articles/10.1186/s42774-020-00038-7`.

[17]   Md. Mehdi Masud Talukder, Md Rukan, and Muhammed Islam. *Comparative Aerodynamic Analysis of Wind Turbine Blade Profiles*. Jan. 2015. DOI: `10.17577/IJERTV5IS010031`.

[18]   E. Vandame. *Wing analysis with APAME*. 2011. URL: `http://www.vandame.eu/tutorials/TUT1102R0.pdf`.

[19]   Wikipedia. *Lift (force)*. Last accessed 7 May 2023. 2023. URL: `https://en.wikipedia.org/wiki/Lift_(force)`.

[20]   Windy.app. *North sea: weather statistics and wind history*. Last accessed 29 April 2023. 2022. URL: `https://windy.app/forecast2/spot/381566/North+sea/statistics`.

# List of Figures

# A Attachment
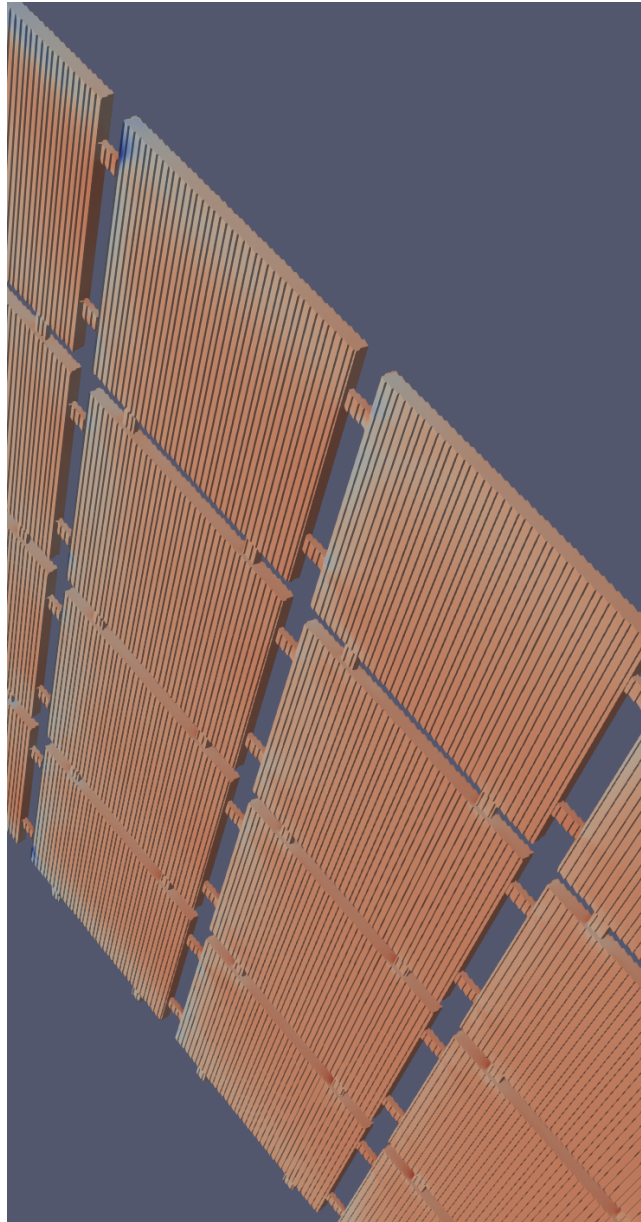
## A.1 Staircase structure

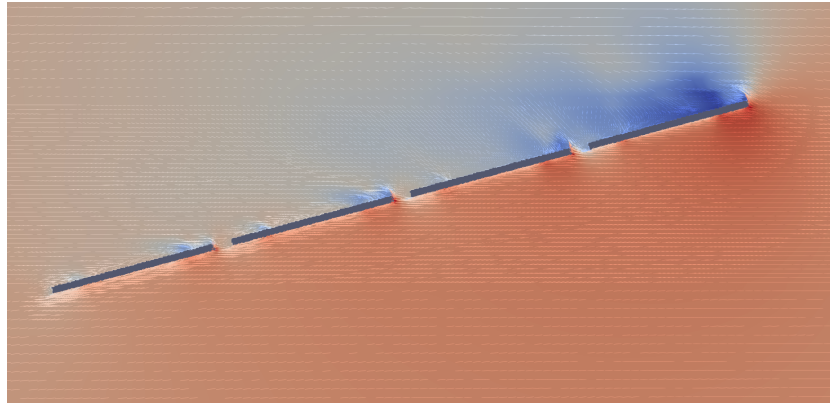

Figure 38

## A.2   CFD Wind plot
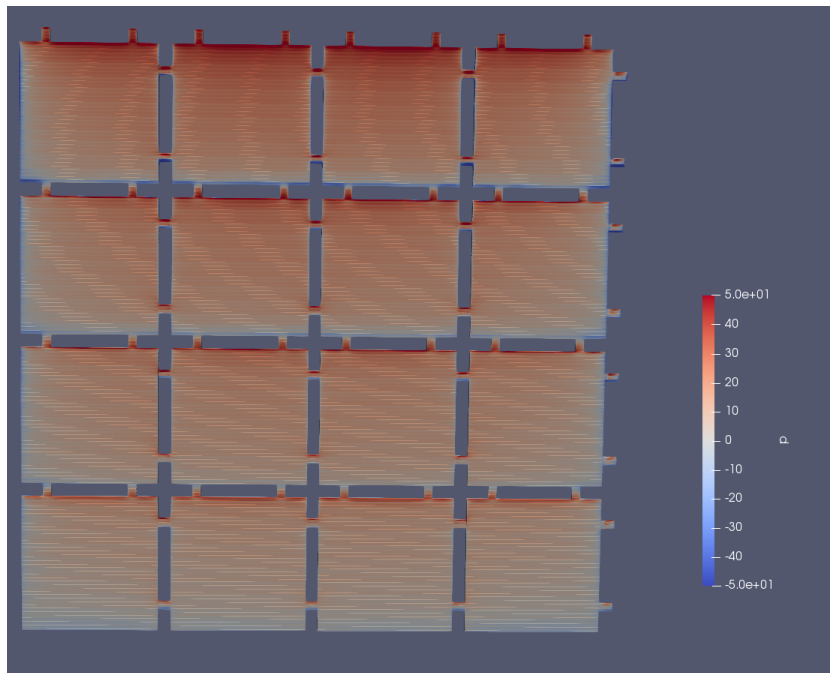


Figure 39

## A.3   CFD Bridges



Figure 40

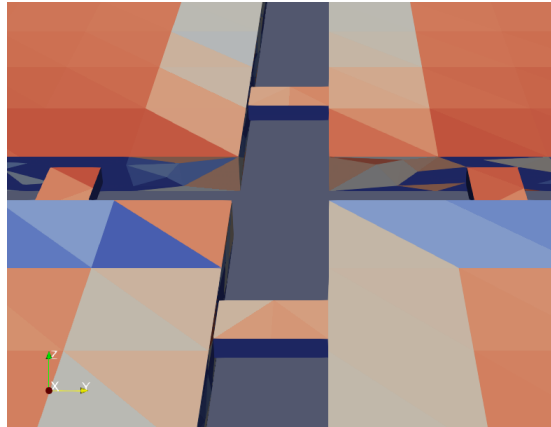## A.4 Pressure on bridges, above angle



Figure 41

## A.5 Pressure on bridges, below angle
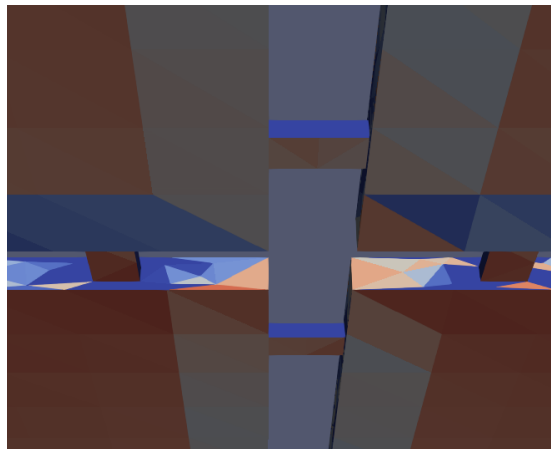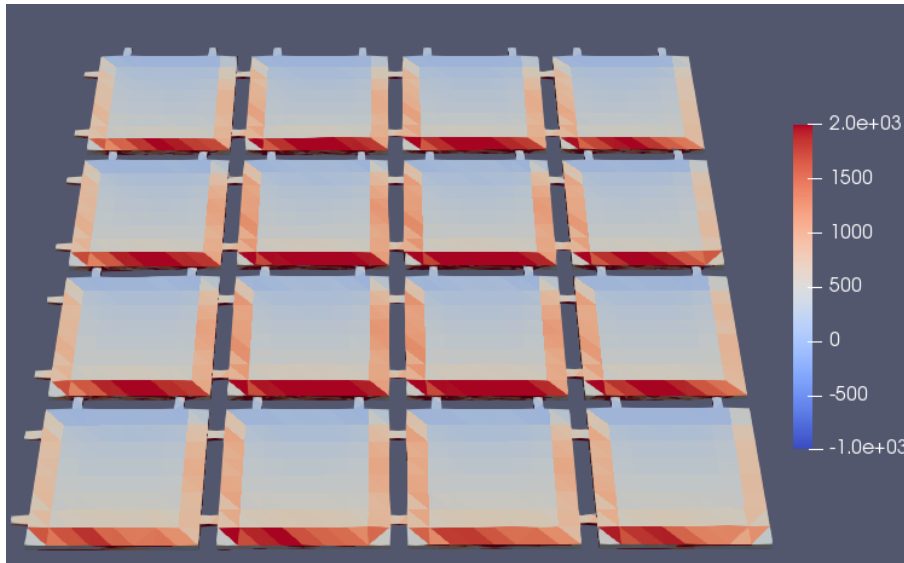


Figure 42

## A.6 Pressure plot at 25 $m/s$, above angle



Figure 43

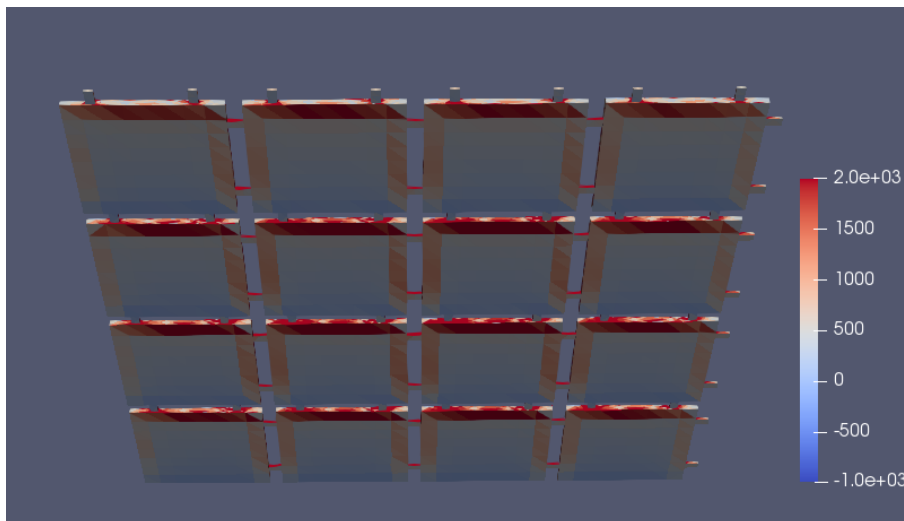## A.7 Pressure on bridges, below angle



Figure 44